

Achieving the continuum limit of quantum link lattice gauge theories on quantum devices

Torsten V. Zache,^{1, 2, 3} Maarten Van Damme,⁴ Jad C. Halimeh,⁵ Philipp Hauke,⁵ and Debasish Banerjee^{6, 7}

¹*Center for Quantum Physics, University of Innsbruck, 6020 Innsbruck, Austria*

²*Institute for Quantum Optics and Quantum Information of the Austrian Academy of Sciences, 6020 Innsbruck, Austria*

³*Heidelberg University, Institut für Theoretische Physik, Philosophenweg 16, 69120 Heidelberg, Germany*

⁴*Department of Physics and Astronomy, University of Ghent, Krijgslaan 281, 9000 Gent, Belgium*

⁵*INO-CNR BEC Center and Department of Physics,*

University of Trento, Via Sommarive 14, I-38123 Trento, Italy

⁶*Saha Institute of Nuclear Physics, HBNI, 1/AF Bidhannagar, Kolkata 700064, India*

⁷*Institut für Physik, Humboldt-Universität zu Berlin,*

Zum Großen Windkanal 6, 12489 Berlin, Germany

(Dated: April 2, 2021)

The solution of gauge theories is one of the most promising applications of quantum technologies. Here, we discuss the approach to the continuum limit for $U(1)$ gauge theories regularized via finite-dimensional Hilbert spaces of quantum spin- S operators, known as quantum link models. For quantum electrodynamics (QED) in one spatial dimension, we numerically demonstrate the continuum limit by extrapolating the ground state energy, the scalar, and the vector meson masses to large spin lengths S , large volume N , and vanishing lattice spacing a . By analytically solving Gauss' law for arbitrary S , we obtain a generalized PXP spin model and count the physical Hilbert space dimension analytically. This allows us to quantify the required resources for reliable extrapolations to the continuum limit on quantum devices. We use a functional integral approach to relate the model with large values of half-integer spins to the physics at topological angle $\Theta = \pi$. Our findings indicate that quantum devices will in the foreseeable future be able to quantitatively probe the QED regime with quantum link models.

Introduction – The rapid development of quantum technologies culminating in the precise control of large quantum systems [1–4] has fundamentally altered the scope of physics questions that can be addressed for strongly interacting systems. As a complementary approach to smashing nuclei in colliders to uncover their substructure, one can realize quantum many-body systems in controlled analog quantum simulators or digital quantum computers, and study their ground state properties at finite density or during real-time evolution associated with quenches, which are extremely difficult to tackle using Markov Chain Monte Carlo methods [5, 6]. Motivated by this possibility, pioneering proposals [7–9] have been put forward to study properties of lattice gauge theories with the long-term goal of simulating quantum chromodynamics (QCD), the theory of strong interactions. These ideas have triggered an intensive theory effort to devise efficient and feasible implementations (for recent reviews see, e.g., [10–12]), resulting in first experimental realizations [13–20] in recent years.

Nonperturbative calculations of quantum field theories (QFTs) require a careful treatment of regularization and renormalization, for which the lattice approach has proven most successful [22]. The lattice Hamiltonian of a gauge theory [23] retains exact gauge invariance while a finite spatial lattice reduces the infinite number of degrees of freedom of the field theory to a finite number of lattice sites and links. The local Hilbert space dimension of the gauge fields, however, remains infinite in the original Wilsonian formulation. Quantum link

models (QLMs) [24–26] regulate these infinite dimensional Hilbert spaces with qudits while maintaining exact gauge invariance and are ideal candidates to be studied on quantum devices such as analog quantum simulators or digital quantum computers. Extracting information relevant for the QFT in the continuum limit, especially when realized in the low-dimensional Hilbert spaces available in current quantum devices, requires a sequence of extrapolations which is the main topic of this article.

Effects of truncating the infinite-dimensional Hilbert space have been extensively investigated for lattice theories with continuous global and local symmetries [27–32]. For pure $U(1)$ gauge theory in $(2+1)$ -d dimensions, truncations in the magnetic basis have been argued to be superior to truncations in the electric basis for reaching the continuum limit [33, 34]. Nevertheless, rapid convergence in such truncations has been observed previously in [35, 36]. The related approach of approximating continuous groups with discrete groups of increasing order also has a long history [37–40].

The continuum limit physics is quite sensitive to the nature of the employed truncation. For example, in the $(1+1)$ -d $O(3)$ model the physics of asymptotic freedom could only be recovered with at least a 16-dimensional local Hilbert space in the angular momentum basis truncation [41]. However, using qubit operators [42], it was shown that the same continuum limit only required 2-qubits per site [43]. The QLM approach is similar to this qubit-regularization, but uses larger spin- S operators for the $U(1)$ gauge links. It was analytically shown

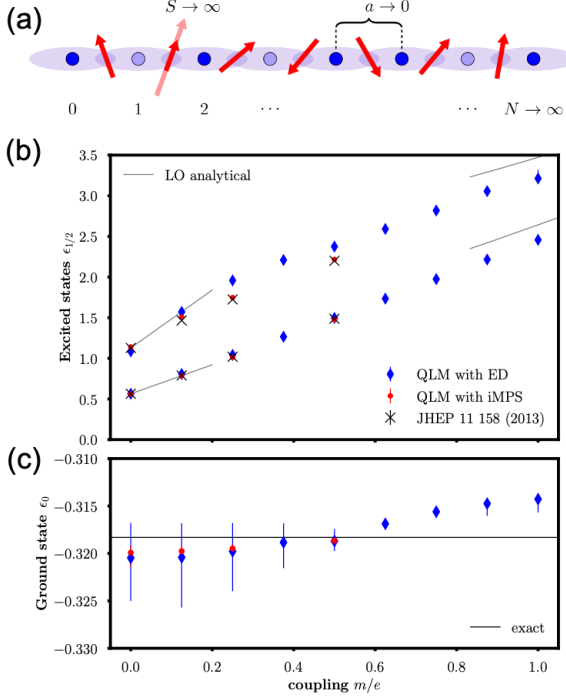


Figure 1. (a) In a U(1) QLM, matter fields (blue dots) reside on the sites of a lattice while gauge fields, represented by spins (red arrows), live on the links connecting two neighboring lattice sites. Gauss' law ties consecutive gauge fields to the matter in between as indicated by the shaded ellipses. The ground state energy, shown in (c), and the first two excited states (with vector and scalar quantum numbers), shown in (b), in the zero momentum sector of QED obtained from the $U(1)$ QLM using ED and iMPS show excellent agreement with the analytical prediction for $m/e = 0$. In (b), the grey solid lines indicate the leading order (LO) analytical expansions [21] for small m/e and e/m , respectively. The error bars indicate an estimated systematic uncertainty (see SM).

that large representations for the gauge links in QLMs recover the standard Wilson lattice gauge theory [44]. A fine-tuning free approach to the continuum limit using the QLMs is via the dimensional reduction in the D-theory formulation [45]. This is, however, only possible if a phase with an exponentially large correlation length is generated [46]. In this article, we explore the former approach and show that careful analysis techniques allow us to reach the continuum limit quantitatively for certain physical observables, even with very small values of S ($\lesssim 3 - 5$), extending the observations made in [35, 36]. We solve the Gauss' law analytically for a general spin- S representation, and estimate the quantum resources to simulate the continuum limit. Further, we use a functional integral representation to demonstrate how large half-integer spins give rise to the topological angle $\Theta = \pi$.

Hamiltonian and Gauss' law – We focus on $U(1)$ gauge theories in d spatial dimensions with (staggered) fermionic matter [23]. The gauge fields are described

by quantum spins $\hat{\mathbf{S}}_{\mathbf{n},j}$ of length S residing on the links (\mathbf{n},j) connecting neighboring sites \mathbf{n} and $\mathbf{n} + \mathbf{e}_j$ on a hypercubic lattice of size N^d . The spins are coupled to fermionic operators $\hat{\psi}_{\mathbf{n}}$ living on the sites, as described by the Hamiltonian

$$\hat{H} = \frac{g^2}{2} \sum_{\mathbf{n},j} (\hat{S}_{\mathbf{n},j}^z)^2 + \mu \sum_{\mathbf{n}} (-1)^{n_1 + \dots + n_d} \hat{\psi}_{\mathbf{n}}^\dagger \hat{\psi}_{\mathbf{n}} - \hat{H}_m - \frac{1}{2\sqrt{S(S+1)}} \sum_{\mathbf{n},j} (-1)^{\sum_{k < j} n_k} (\hat{\psi}_{\mathbf{n}}^\dagger \hat{S}_{\mathbf{n},j}^+ \hat{\psi}_{\mathbf{n} + \mathbf{e}_j} + \text{H.c.}) . \quad (1)$$

The first term is the electric field energy at the bare coupling g , and the second term sets the staggered fermion mass μ . The gauge-matter interaction is the correlated hopping of fermions along a link with the simultaneous raising or lowering of the corresponding spin. For $d > 1$, there is the magnetic energy term, $\hat{H}_m = \frac{1}{2g^2S^2(S+1)^2} \sum_P (\hat{S}_{P_1}^+ \hat{S}_{P_2}^+ \hat{S}_{P_3}^- \hat{S}_{P_4}^- + \text{h.c.})$, with P labeling elementary plaquettes consisting of links $P_{1,2,3,4}$ forming a square. The gauge fields U, U^\dagger and the electric field E are represented by S^+, S^- and S^z operators, respectively. They satisfy the commutation relations, $[E, U^{(\dagger)}] = (-)U^{(\dagger)}$, and preserve an exact gauge symmetry with $(2S+1)$ -dimensional Hilbert space. To achieve the correct scaling behavior, appropriate factors of S are inserted in the dimensionless couplings in Eq. (1) (see SM for more details). The gauge transformations are generated by the Gauss' law operator,

$$\hat{G}_{\mathbf{n}} = \sum_j (\hat{S}_{\mathbf{n} + \mathbf{e}_j, j}^z - \hat{S}_{\mathbf{n}, j}^z) - \left[\frac{(-1)^{\mathbf{n}} - 1}{2} + \hat{\psi}_{\mathbf{n}}^\dagger \hat{\psi}_{\mathbf{n}} \right] , \quad (2)$$

which satisfy $[\hat{H}, \hat{G}_{\mathbf{n}}] = 0$. The Hilbert space thus separates into superselection sectors labelled by eigenvalues of $\hat{G}_{\mathbf{n}}$. In the absence of static charges, states in the physical Hilbert space, $\mathcal{H}_{\text{phys}}$, satisfy $\hat{G}_{\mathbf{n}}|\text{phys}\rangle = 0$.

In the renormalization group (RG) sense, the parameters g , μ , and S can be regarded as directions in the space of couplings, to be adjusted such that the theory flows to a fixed point corresponding to the desired QFT. In the remainder of this letter, we focus on the case of one spatial dimension, $d = 1$, where Eq. (1) provides a lattice version of the (massive) Schwinger model [47–49]. The continuum Schwinger model is parameterized by the (bare) values of the electric charge e and the fermion mass m . In its lattice version at lattice spacing a , these parameters appear through the dimensionless combinations $g = ae$ and $\mu = am$. The QFT limit is reached for large S , large N , and small a , as demonstrated numerically in Fig. 1(a). Specifically, we first take the infinite spin length limit $S \rightarrow \infty$ at fixed a and N ; then the thermodynamic limit $N \rightarrow \infty$ at fixed a ; and finally the continuum limit $a \rightarrow 0$ at fixed μ/g . The different extrapolations have to be performed for appropriately rescaled

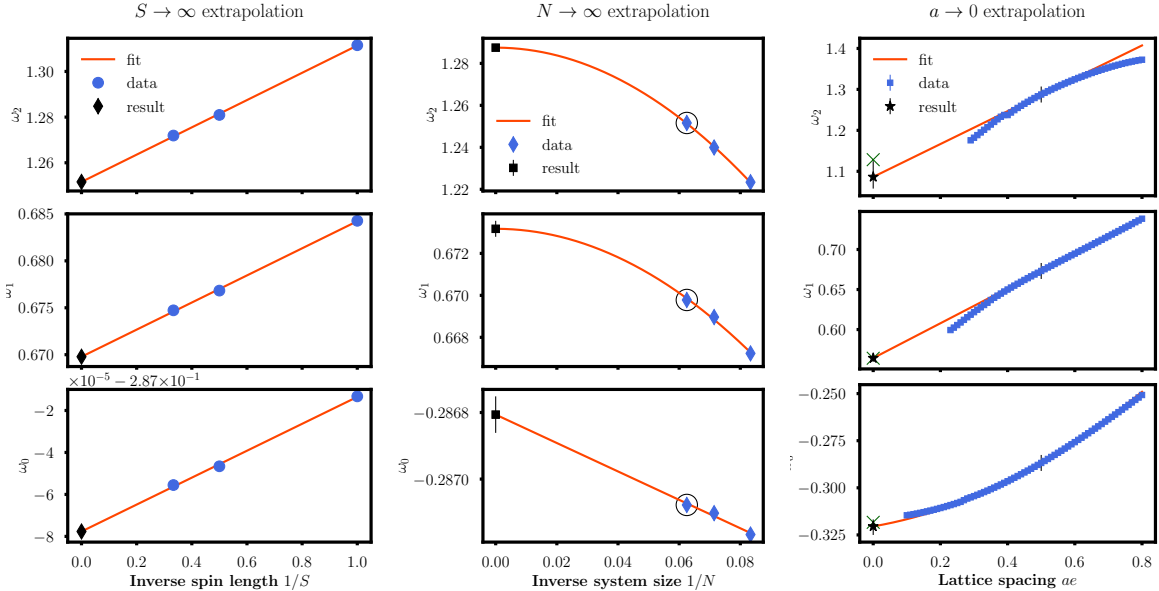


Figure 2. We illustrate the sequence of extrapolations, in the panels from the left to the right, required to reach the continuum limit for the ED data with $m/e = 0$. The energies of the vacuum (bottom row), vector particle (middle row), and scalar particle (top row) are extrapolated to $S \rightarrow \infty$ (left column), $N \rightarrow \infty$ (middle column), and $a \rightarrow 0$ (right column), as discussed in the main text. The circles in the middle row indicate the values obtained from the corresponding S -extrapolations shown in the left column. Similarly, the ticks in the right column indicate the values corresponding to the N -extrapolations in the middle column. For clarity, we only show selected values of ae and N for the first two extrapolations. For comparison, the green crosses indicate the exact analytical results.

(“renormalized”) quantities that correspond to physical observables (see the SM for details). In general, the final continuum limit involves a rescaling of the dimensionless coupling constants in order to reach the RG fixed point [22]. This complication is absent for the present model (except for a redefinition of the ground state energy) [48, 50].

Mass spectrum from the QLM – The massive Schwinger model is considerably simpler than QED in two or three dimensions due to the absence of magnetic interactions and the strong constraints of Gauss’ law. As a consequence, both the weak and strong coupling limits, $e/m = 0$ and $e/m = \infty$, respectively, are exactly solvable, and analytic expansions around these limits [21, 51] can be used for benchmarking the extrapolation. Our principal numerical methods are exact diagonalization (ED) (using the Python package QuSpin [52]) and variational techniques based on infinite Matrix Product States (iMPS) [53, 54] directly in the thermodynamic limit. To perform ED, we derive an equivalent spin model constrained by a projector \mathcal{P} on neighboring gauge link configurations allowed by Gauss’ law. The resulting Hamiltonian has the form (see SM):

$$\hat{H} = \mathcal{P} \sum_{n=1}^N \left\{ \frac{g^2}{2} (\hat{S}_n^z)^2 + 2\mu(-1)^n \hat{S}_n^z - \frac{\hat{S}_n^x}{\sqrt{S(S+1)}} \right\} \mathcal{P}. \quad (3)$$

For $S = 1/2$, this reduces to a constrained model of hardcore bosons [55], sometimes referred to as PXP model, whose total number of allowed states can be analytically counted [56], and is believed to be the simplest model to explain the anomalous thermalization observed in the 51-Rydberg atom experiment [57]. Extending the analysis in [56], we derive an analytic expression for the dimension of the physical Hilbert subspace, given by (see SM)

$$\dim \mathcal{H}_{\text{phys}}(S, N) = 2^N \sum_{m=1}^{2S+1} \left[\cos \left(\frac{m\pi}{4S+3} \right) \right]^N. \quad (4)$$

The remarkably small Hilbert space size, scaling linearly with S at a fixed N , enables ED calculations for relatively large system sizes, and data up to $S = 3$ and $N = 16$ is presented here. Results from iMPS simulations in the thermodynamic limit are also shown for $S \leq 5$ for the Hamiltonian in Eq. (1), where Gauss’ law is enforced by adding a large energy penalty $\propto \sum_{\mathbf{n}} \hat{G}_{\mathbf{n}}^2$ [58, 59]. Our results, summarized in Fig. 1, demonstrate how to accurately reach the continuum limit with QLMs for the ground state energy and the energies of the first two excited states, the “vector” and “scalar” particles. We find excellent agreement in the strong coupling limit, due to small fluctuations around $\langle \hat{S}^z \rangle = 0$, such that our numerics with small S (≤ 3 for ED and ≤ 5 for iMPS) already capture the relevant physics. For higher excited states or towards weak coupling, the fluctuations grow more pro-

nounced and larger spin lengths S become necessary.

The detailed steps of the underlying extrapolation are shown in Fig. 2 for ED, illustrated for the analytically solvable strong-coupling limit ($m/e = 0$). Despite the small spin lengths $S = 1, 2, 3$, we observe a clear $1/S$ scaling, enabling a reliable extrapolation to the $S \rightarrow \infty$ limit. Similarly, the subsequent $N \rightarrow \infty$ extrapolation is performed with the expected leading behavior at large N . The largest systematic error arises from the choice of fit range for the final $a \rightarrow 0$ extrapolation. The latter is complicated because the parameters close to the continuum limit (small a) require increasingly large values of N and S , which we attribute to increasing electric field fluctuations. Empirically, we find that systematic errors are minimized by disregarding “far-off” N and S extrapolation where the extrapolated values differ by more than 10% from the one of the largest available system size. We thus select a smallest lattice spacing a for which the underlying data is sufficiently converged with respect to S and N . Note that this procedure naturally depends on the observable. The ground state energy can be extrapolated with lattice spacings down to $ae \sim 0.1$, while we only reach $ae \sim 0.3$ for the scalar mass. For a detailed discussion of the numerical extrapolations, we refer to the SM.

Figure 3 shows our final results for the vector and scalar masses with a trivial m/e dependence subtracted. The iMPS results are obtained analogously to the ED simulations, but without the N extrapolation. The agreement between both approaches demonstrates that our extrapolations indeed reach the thermodynamic limit, and that the limits $S \rightarrow \infty$ and $N \rightarrow \infty$ commute for this model. Comparing to previously obtained results [60], which effectively correspond to $S \rightarrow \infty$, we find good agreement of both the ED and iMPS data for the vector mass, indicating that $S = 3$ is sufficient to resolve this excitation. As anticipated, the scalar mass requires larger values of S , and we observe stronger deviations in ED.

Estimation of required resources on a quantum device

– As illustrated above, already very small spin lengths $S \lesssim 3$ and system sizes $N \lesssim 16$ are sufficient to obtain quantitative estimates for the low-lying mass spectrum. A brute-force implementation would nevertheless still require controlling a Hilbert space of dimension $[2(2S+1)]^N \sim 14^{16}$, approximately equal to that of 61 unconstrained qubits. Due to Gauss’ law, most of these states are unnecessary.

To estimate the minimal required resources to implement the model on a quantum device, consider the equivalent spin model, Eq. (3). Suppose a quantum device could naturally work with the corresponding qudits of size $2S+1$ [61–68]. Then control over only $N \sim 16$ such degrees of freedom would be sufficient to reach the continuum limit. According to Eq. (4), a perfect encoding on a digital quantum computer would need only

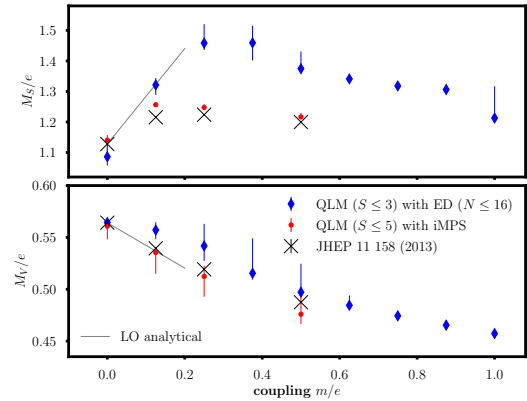


Figure 3. Final result for vector (lower panel) and scalar (upper panel) masses, with the leading dependence $2m/e$ subtracted. Our results reproduce the analytic prediction of the massless limit ($m/e = 0$) and are quantitatively consistent with the perturbative expectation (grey solid line). For the vector mass, both iMPS (red dots) and ED (blue diamonds) results agree with each other and previously obtained results (black crosses) at infinite spin length. As expected, the scalar mass requires larger values of S , leading to stronger deviations of the ED data.

$\dim \mathcal{H}_{\text{phys}}(S = 3, N = 16) = 63757 < 2^{16}$ states. We thus conclude that our procedure may be carried out on existing quantum computing devices with control over 16 qubits. This fact has been already exploited to carry out the ED calculations on a conventional laptop computer.

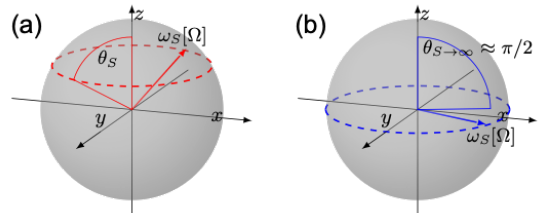


Figure 4. (a) Closed path traced by a quantum spin- S on the Bloch sphere; (b) with increasing S , the path of the spin is forced along the equator to minimize fluctuations of the electric energy term.

Coherent State Path Integral – Coherent state path integrals can explain the approach to the Kogut-Susskind limit for large- S values. A spin- S located at spatial site \mathbf{n} traces out an arbitrary closed curve on the Bloch sphere under the Hamiltonian evolution in imaginary time subtending a solid angle Ω , as shown in Fig. 4(a). In the corresponding expression of the path integral (see SM), the electric field squared $(\hat{S}_{\mathbf{n}}^z)^2$ term contributes as $\sim \exp[-\epsilon g^2 S(S-1/2) \cos^2(\theta_{\mathbf{n}})/2]$, where ϵ is the Trotter discretization and $\theta_{\mathbf{n}}, \phi_{\mathbf{n}}$ are the angular coordinates of the spin. For large $g^2 S$, the minimization of this quadratic term yields $\theta_{\mathbf{n}} \rightarrow \pi/2$ as indicated in Fig. 4(b). In this limit, the quantum spin is confined to the equator

of the Bloch sphere and resembles the quantum rotor of the Wilson-Kogut-Susskind formulation, consistent with the numerics.

An important additional observation is that the area traced out by the closed curve on the Bloch sphere by $\hat{\mathbf{S}}_n$ admits a topological interpretation as a Berry phase. In the continuum limit, this area is $\omega[\Omega] = \int_0^\beta d\tau \dot{\phi}(\tau) \cos(\theta(\phi(\tau))) = \oint_{\phi_0} d\phi \cos(\theta(\phi))$ [69], where $\tau \in [0, \beta]$ is the Euclidean time. At leading order in the large- S limit, only the number of total windings is relevant, with each winding contributing $2\pi S$. While this term is irrelevant for the integer spins used in this work, for half-integer spins it gives rise to a π -flux in the system. This feature rigorously establishes that QLMs with large values of half-integer spin lead to a topological theta angle $\Theta = \pi$, often anticipated in the literature [9, 18, 70, 71] already for the spin-1/2 case.

Conclusion and outlook – In this paper, we have numerically demonstrated the continuum limit of QED in $(1+1)$ -d, regularized with quantum spin- S operators for several physical observables. A highlight of our results — made possible by systematic finite size scalings and careful continuum extrapolations — are the small spin values $S \lesssim 3 - 5$ that suffice to reach the continuum limit. The systematic finite size scaling enables us to quantitatively estimate the resources of a quantum device to realize the continuum limit. These results lend hope that near future quantum simulation experiments with small S and limited lattice size can yield valuable data that can be extrapolated to the QFT limit. Using a coherent state path integral, the approach to the Kogut-Susskind limit is derived and the connection of half-integer spins with topological angle π is formalized.

Our results point to several directions for future investigations. Remaining in $(1+1)$ -d, an immediate question concerns the existence of new critical points in the phase diagram with half-integer spins, and other values of the couplings μ/g . The mapping to generalized PXP model begets the question if quantum scars, responsible for anomalous thermalization in the PXP model, are also present in the higher spin representations [72]. The Floquet dynamics of such models also have a rich phase structure [73, 74] and are worth studying. Going to higher dimensions, an exciting challenge is to figure out whether the convergence properties of both Abelian and non-Abelian QLMs with increasing link representations are equally efficient as in one spatial dimension.

ACKNOWLEDGMENTS

We thank Shailesh Chandrasekharan, Robert Ott, Arnab Sen, and Uwe-Jens Wiese for useful discussions. This work was supported by the Simons Collaboration on UltraQuantum Matter, which is a grant from the Simons Foundation (651440, P.Z.). D.B. acknowledges sup-

port by the German Research Foundation (DFG), Grant ID BA 5847/2-1. This work is part of and supported by the Interdisciplinary Center Q@TN — Quantum Science and Technologies at Trento, the DFG Collaborative Research Centre SFB 1225 (ISOQUANT), the Provincia Autonoma di Trento, and the ERC Starting Grant StrEnQTh (Project- ID 804305).

- [1] I. Bloch, J. Dalibard, and S. Nascimbène, *Nature Physics* **8**, 267 (2012).
- [2] R. Blatt and C. F. Roos, *Nature Physics* **8**, 277 (2012).
- [3] I. M. Georgescu, S. Ashhab, and F. Nori, *Reviews of Modern Physics* **86**, 153 (2014).
- [4] P. Hauke, F. M. Cucchietti, L. Tagliacozzo, I. Deutsch, and M. Lewenstein, *Reports on Progress in Physics* **75**, 082401 (2012).
- [5] W. Hofstetter and T. Qin, *Journal of Physics B: Atomic, Molecular and Optical Physics* **51**, 082001 (2018).
- [6] U.-J. Wiese, *Nuclear Physics A* **931**, 246–256 (2014).
- [7] E. Zohar, J. I. Cirac, and B. Reznik, *Phys. Rev. Lett.* **109**, 125302 (2012), arXiv:1204.6574 [quant-ph].
- [8] L. Tagliacozzo, A. Celi, A. Zamora, and M. Lewenstein, *Annals Phys.* **330**, 160 (2013), arXiv:1205.0496 [cond-mat.quant-gas].
- [9] D. Banerjee, M. Dalmonte, M. Muller, E. Rico, P. Strelber, U. J. Wiese, and P. Zoller, *Phys. Rev. Lett.* **109**, 175302 (2012), arXiv:1205.6366 [cond-mat.quant-gas].
- [10] E. Zohar, J. I. Cirac, and B. Reznik, *Reports on Progress in Physics* **79**, 014401 (2015).
- [11] M. Dalmonte and S. Montangero, *Contemporary Physics* **57**, 388 (2016), <https://doi.org/10.1080/00107514.2016.1151199>.
- [12] M. C. Banuls, R. Blatt, J. Catani, A. Celi, J. I. Cirac, M. Dalmonte, L. Fallani, K. Jansen, M. Lewenstein, S. Montangero, *et al.*, *The European physical journal D* **74**, 1 (2020).
- [13] E. A. Martinez, C. A. Muschik, P. Schindler, D. Nigg, A. Erhard, M. Heyl, P. Hauke, M. Dalmonte, T. Monz, P. Zoller, *et al.*, *Nature* **534**, 516 (2016).
- [14] N. Klco, E. F. Dumitrescu, A. J. McCaskey, T. D. Morris, R. C. Pooser, M. Sanz, E. Solano, P. Lougovski, and M. J. Savage, *Physical Review A* **98**, 032331 (2018).
- [15] C. Schweizer, F. Grusdt, M. Berngruber, L. Barbiero, E. Demler, N. Goldman, I. Bloch, and M. Aidelsburger, *Nature Physics* **15**, 1168 (2019).
- [16] F. Görg, K. Sandholzer, J. Minguzzi, R. Desbuquois, M. Messer, and T. Esslinger, *Nature Physics* **15**, 1161 (2019).
- [17] A. Mil, T. V. Zache, A. Hegde, A. Xia, R. P. Bhatt, M. K. Oberthaler, P. Hauke, J. Berges, and F. Jendrzejewski, *Science* **367**, 1128 (2020).
- [18] B. Yang, H. Sun, R. Ott, H.-Y. Wang, T. V. Zache, J. C. Halimeh, Z.-S. Yuan, P. Hauke, and J.-W. Pan, arXiv preprint arXiv:2003.08945 (2020).
- [19] Y. Atas, J. Zhang, R. Lewis, A. Jahanpour, J. F. Haase, and C. A. Muschik, arXiv preprint arXiv:2102.08920 (2021).
- [20] H.-H. Lu, N. Klco, J. M. Lukens, T. D. Morris, A. Bansal, A. Ekström, G. Hagen, T. Papenbrock, A. M. Weiner,

M. J. Savage, and et al., *Physical Review A* **100** (2019), [10.1103/physreva.100.012320](https://doi.org/10.1103/physreva.100.012320).

[21] P. Srianesh, C. Hamer, and R. Bursill, *Physical Review D* **62**, 034508 (2000).

[22] I. Montvay and G. Münster, *Quantum fields on a lattice* (Cambridge University Press, 1997).

[23] J. Kogut and L. Susskind, *Physical Review D* **11**, 395 (1975).

[24] D. Horn, *Phys. Lett. B* **100**, 149 (1981).

[25] P. Orland and D. Rohrlich, *Nucl. Phys. B* **338**, 647 (1990).

[26] S. Chandrasekharan and U.-J. Wiese, *Nuclear Physics B* **492**, 455 (1997).

[27] T. Byrnes, P. Srianesh, R. J. Bursill, and C. J. Hamer, *Phys. Rev. D* **66**, 013002 (2002), [arXiv:hep-lat/0202014](https://arxiv.org/abs/hep-lat/0202014).

[28] T. Byrnes and Y. Yamamoto, *Phys. Rev. A* **73**, 022328 (2006), [arXiv:quant-ph/0510027](https://arxiv.org/abs/quant-ph/0510027).

[29] D. Yang, G. S. Giri, M. Johanning, C. Wunderlich, P. Zoller, and P. Hauke, *Phys. Rev. A* **94**, 052321 (2016).

[30] B. Buyens, S. Montangero, J. Haegeman, F. Verstraete, and K. Van Acoleyen, *Physical Review D* **95** (2017), [10.1103/physrevd.95.094509](https://doi.org/10.1103/physrevd.95.094509).

[31] F. Niedermayer and U. Wolff, *PoS LATTICE2016*, 317 (2016), [arXiv:1612.00621 \[hep-lat\]](https://arxiv.org/abs/1612.00621).

[32] I. Raychowdhury and J. R. Stryker, *Phys. Rev. Res.* **2**, 033039 (2020), [arXiv:1812.07554 \[hep-lat\]](https://arxiv.org/abs/1812.07554).

[33] D. B. Kaplan and J. R. Stryker, *Phys. Rev. D* **102**, 094515 (2020), [arXiv:1806.08797 \[hep-lat\]](https://arxiv.org/abs/1806.08797).

[34] D. Paulson *et al.*, (2020), [arXiv:2008.09252 \[quant-ph\]](https://arxiv.org/abs/2008.09252).

[35] S. Kühn, J. I. Cirac, and M.-C. Bañuls, *Physical Review A* **90**, 042305 (2014).

[36] B. Buyens, S. Montangero, J. Haegeman, F. Verstraete, and K. Van Acoleyen, *Physical Review D* **95**, 094509 (2017).

[37] G. Bhanot and C. Rebbi, *Phys. Rev. D* **24**, 3319 (1981).

[38] P. Hasenfratz and F. Niedermayer, *Nucl. Phys. B* **596**, 481 (2001), [arXiv:hep-lat/0006021](https://arxiv.org/abs/hep-lat/0006021).

[39] E. Ercolessi, P. Facchi, G. Magnifico, S. Pascazio, and F. V. Pepe, *Phys. Rev. D* **98**, 074503 (2018), [arXiv:1705.11047 \[quant-ph\]](https://arxiv.org/abs/1705.11047).

[40] A. Alexandru, P. F. Bedaque, S. Harmalkar, H. Lamm, S. Lawrence, and N. C. Warrington (NuQS), *Phys. Rev. D* **100**, 114501 (2019), [arXiv:1906.11213 \[hep-lat\]](https://arxiv.org/abs/1906.11213).

[41] F. Bruckmann, K. Jansen, and S. Kühn, *Phys. Rev. D* **99**, 074501 (2019), [arXiv:1812.00944 \[hep-lat\]](https://arxiv.org/abs/1812.00944).

[42] H. Singh and S. Chandrasekharan, *Phys. Rev. D* **100**, 054505 (2019), [arXiv:1905.13204 \[hep-lat\]](https://arxiv.org/abs/1905.13204).

[43] T. Bhattacharya, A. J. Buser, S. Chandrasekharan, R. Gupta, and H. Singh, (2020), [arXiv:2012.02153 \[hep-lat\]](https://arxiv.org/abs/2012.02153).

[44] B. Schlittgen and U. J. Wiese, *Phys. Rev. D* **63**, 085007 (2001), [arXiv:hep-lat/0012014](https://arxiv.org/abs/hep-lat/0012014).

[45] R. Brower, S. Chandrasekharan, S. Riederer, and U. J. Wiese, *Nucl. Phys. B* **693**, 149 (2004), [arXiv:hep-lat/0309182](https://arxiv.org/abs/hep-lat/0309182).

[46] B. B. Beard, M. Pepe, S. Riederer, and U. J. Wiese, *Phys. Rev. Lett.* **94**, 010603 (2005), [arXiv:hep-lat/0406040](https://arxiv.org/abs/hep-lat/0406040).

[47] J. Schwinger, *Phys. Rev.* **128**, 2425 (1962).

[48] S. R. Coleman, R. Jackiw, and L. Susskind, *Annals Phys.* **93**, 267 (1975).

[49] S. R. Coleman, *Annals Phys.* **101**, 239 (1976).

[50] E. Abdalla, M. C. B. Abdalla, and K. D. Rothe, *Non-perturbative methods in 2 dimensional quantum field theory* (World Scientific, 1991).

[51] C. J. Hamer, W.-h. Zheng, and J. Oitmaa, *Phys. Rev. D* **56**, 55 (1997), [arXiv:hep-lat/9701015](https://arxiv.org/abs/hep-lat/9701015).

[52] P. Weinberg and M. Bukov, *SciPost Phys.* **7**, 97 (2019).

[53] V. Zauner-Stauber, L. Vanderstraeten, M. T. Fishman, F. Verstraete, and J. Haegeman, *Physical Review B* **97**, 045145 (2018).

[54] J. Haegeman, B. Pirvu, D. J. Weir, J. I. Cirac, T. J. Osborne, H. Verschelde, and F. Verstraete, *Physical Review B* **85**, 100408 (2012).

[55] P. Fendley, K. Sengupta, and S. Sachdev, *Phys. Rev. B* **69**, 075106 (2004).

[56] C. J. Turner, A. A. Michailidis, D. A. Abanin, M. Serbyn, and Z. Papić, *Nature Physics* **14**, 745 (2018).

[57] H. Bernien, S. Schwartz, A. Keesling, H. Levine, A. Omran, H. Pichler, S. Choi, A. S. Zibrov, M. Endres, M. Greiner, *et al.*, *Nature* **551**, 579 (2017).

[58] J. C. Halimeh and P. Hauke, *Phys. Rev. Lett.* **125**, 030503 (2020).

[59] M. V. Damme, J. C. Halimeh, and P. Hauke, (2020), [arXiv:2010.07338 \[cond-mat.quant-gas\]](https://arxiv.org/abs/2010.07338).

[60] M. C. Bañuls, K. Cichy, J. I. Cirac, and K. Jansen, *Journal of High Energy Physics* **2013**, 158 (2013).

[61] V. Kasper, D. González-Cuadra, A. Hegde, A. Xia, A. Dauphin, F. Huber, E. Tiemann, M. Lewenstein, F. Jendrzejewski, and P. Hauke, (2020), [arXiv:2010.15923 \[cond-mat.quant-gas\]](https://arxiv.org/abs/2010.15923).

[62] Y. Wang, Z. Hu, B. C. Sanders, and S. Kais, *Frontiers in Physics* **8**, 479 (2020).

[63] E. Kiktenko, A. Fedorov, A. Strakhov, and V. Man'ko, *Physics Letters A* **379**, 1409–1413 (2015).

[64] F. Moro, A. J. Fielding, L. Turyanska, and A. Patanè, *Advanced Quantum Technologies* **2**, 1900017 (2019), <https://onlinelibrary.wiley.com/doi/pdf/10.1002/qute.201900017>.

[65] P. Imany, M. Alshaykh, J. Lukens, J. A. Jaramillo-Villegas, A. J. Moore, D. E. Leaird, and A. M. Weiner, (2019).

[66] S. Wang, Z.-Q. Yin, H. F. Chau, W. Chen, C. Wang, G.-C. Guo, and Z.-F. Han, *Quantum Science and Technology* **3**, 025006 (2018).

[67] B. E. Mischuck, S. T. Merkel, and I. H. Deutsch, *Phys. Rev. A* **85**, 022302 (2012).

[68] E. O. Kiktenko, A. S. Nikolaeva, P. Xu, G. V. Shlyapnikov, and A. K. Fedorov, *Phys. Rev. A* **101**, 022304 (2020).

[69] M. V. Berry, *Proceedings of the Royal Society of London Series A* **392**, 45 (1984).

[70] P. Hauke, D. Marcos, M. Dalmonte, and P. Zoller, *Physical Review X* **3** (2013), [10.1103/physrevx.3.041018](https://doi.org/10.1103/physrevx.3.041018).

[71] F. M. Surace, P. P. Mazza, G. Giudici, A. Lerose, A. Gambassi, and M. Dalmonte, *Physical Review X* **10**, 021041 (2020).

[72] W. W. Ho, S. Choi, H. Pichler, and M. D. Lukin, *Physical review letters* **122**, 040603 (2019).

[73] B. Mukherjee, S. Nandy, A. Sen, D. Sen, and K. Sengupta, *Phys. Rev. B* **101**, 245107 (2020).

[74] B. Mukherjee, A. Sen, D. Sen, and K. Sengupta, *Phys. Rev. B* **102**, 075123 (2020).

[75] F. Haldane, *Physics Letters A* **93**, 464 (1983).

[76] J. Villain, *J. Phys. (France)* **36**, 581 (1975).

SUPPLEMENTAL MATERIAL

Spin length and lattice units in the QLM – Throughout the main text, we work with units where the speed of light and the Planck constant are set to one, $c = \hbar = 1$. In standard lattice QED, all quantities are rescaled with the lattice spacing a to become dimensionless. For example, the dimensionless coupling is given by $g^2 = e^2 a^{3-d}$, where e is the bare value of the electric charge in d spatial dimensions, and $\mu = am$ with the bare mass m . Similarly, the Hamiltonian is rescaled as $H_{\text{lat}} = aH_{\text{phys}}$ and the fermion operators are related by $\psi_{\text{lat}} = a^{d/2}\psi_{\text{phys}}$, such that $\{(\psi_{\text{lat}})_{\mathbf{n}}, (\psi_{\text{lat}})_{\mathbf{m}}^\dagger\} = \delta_{\mathbf{n}, \mathbf{m}}$.

In the QLM, dimensionless gauge fields are further replaced by spin operators. Explicitly, the electric field $E_{\text{lat}} = a^{d-1}/eE_{\text{phys}}$ and the compact $U(1)$ link operator $U_{\text{lat}} = e^{iaeA_{\text{phys}}}$ are replaced according to

$$E_{\text{lat}} \leftrightarrow S^z, \quad U_{\text{lat}} \leftrightarrow \frac{1}{\sqrt{S(S+1)}} S^+. \quad (5)$$

These identifications are consistent with the canonical commutation relations in the continuum, $[A_{\text{phys}}(\mathbf{x}), E_{\text{phys}}(\mathbf{y})] = i\delta(\mathbf{x} - \mathbf{y})$. Crucially, the explicit appearance of the spin length S ensures the lattice commutation relations $[E_{\text{lat}}, U_{\text{lat}}] = U_{\text{lat}}$ and $[U_{\text{lat}}, U_{\text{lat}}^\dagger] = 0$ in the limit $S \rightarrow \infty$. To see this, consider the operator $e^{i\varphi_S}$ which fulfills $[S^z, e^{i\varphi_S}] = e^{i\varphi_S}$ exactly [75], given by

$$e^{i\varphi_S} = (S + S^z)^{-1/2} S^+ (S - S^z)^{-1/2} \quad (6)$$

$$= \frac{1}{S} \left(1 - \frac{1}{2S} + \frac{1}{8S^2} \right) S^+ \\ + \frac{1}{S^3} \left[(S^z)^2 S^+ - S^+ (S^z)^2 \right] + \dots, \quad (7)$$

where the omitted terms are formally suppressed for $S \gg S^z$. Since $[S(S+1)]^{-1/2} = \frac{1}{S} (1 - \frac{1}{2S}) + \mathcal{O}(1/S^3)$, the normalization given in Eq. (1) captures the correct behavior for large S .

Equivalent spin model and Hilbert space dimension – We derive the effective spin model starting from Eq. (1) in one dimension, i.e.

$$\hat{H} = \sum_{j=1}^N \left[\frac{g^2}{2} (\hat{S}_j^z)^2 + \mu(-1)^j \hat{\psi}_j^\dagger \hat{\psi}_j \right. \\ \left. + \frac{1}{2\sqrt{S(S+1)}} (\hat{\psi}_j^\dagger \hat{S}_j^+ \hat{\psi}_{j+1} + \text{h.c.}) \right], \quad (8)$$

where we take N to be even and assume periodic boundary conditions. The Hamiltonian is gauge invariant, $[\hat{H}, \hat{G}_j] = 0$ with $\hat{G}_j = \hat{S}_j^z - \hat{S}_{j-1}^z - [\hat{\psi}_j^\dagger \hat{\psi}_j + \frac{(-1)^j - 1}{2}]$, and the total fermion number is conserved, $[\hat{H}, \hat{N}_f] = 0$ with $\hat{N}_f = \sum_{j=1}^N \hat{\psi}_j^\dagger \hat{\psi}_j$.

Performing a Jordan-Wigner transformation,

$$\hat{\psi}_j = \hat{\sigma}_j^- \prod_{k=1}^{j-1} \hat{\sigma}_k^z, \quad \hat{\psi}_j^\dagger \hat{\psi}_j = \frac{1}{2} (1 + \hat{\sigma}_j^z), \quad (9)$$

we obtain the equivalent Hamiltonian

$$\hat{H} = \sum_{j=1}^N \left[\frac{g^2}{2} (\hat{S}_j^z)^2 + \frac{\mu}{2} (-1)^j \hat{\sigma}_j^z \right] \\ - \frac{1}{2\sqrt{S(S+1)}} \sum_{j=1}^{N-1} (-1)^{\hat{\alpha}_j} (\hat{\sigma}_j^+ \hat{S}_j^+ \hat{\sigma}_{j+1}^- + \text{h.c.}), \quad (10)$$

where $\hat{\alpha}_j = \hat{N}_f$ for $j = N$ and zero otherwise. The full Hilbert space $\mathcal{H} = \mathcal{H}_S \otimes \mathcal{H}_\sigma$ has dimension $\dim \mathcal{H} = (2S(S+1))^{2N}$, but the physical Hilbert space $\mathcal{H}_{\text{phys}} = \mathcal{H}|_{G_n=0} = \{|\text{phys}\rangle \in \mathcal{H} \mid G_n|\text{phys}\rangle = 0\}$ is much smaller.

Within $\mathcal{H}_{\text{phys}}$, the configurations of $\hat{\sigma}$ are uniquely determined by those of \hat{S} and thus we can express all operators in $\mathcal{H}_{\text{phys}}$ in terms of \hat{S} . Let \mathcal{P} be the operator that projects all possible spin configurations in \mathcal{H}_S to the allowed ones in $\mathcal{H}_{\text{phys}}$. Employing $\hat{S}_j^z - \hat{S}_{j-1}^z = \frac{1}{2} [\hat{\sigma}_j^z + (-1)^j]$ on the physical subspace and shifting indices, we find

$$\hat{H} = \mathcal{P} \sum_{j=1}^N \left[\frac{g^2}{2} (\hat{S}_j^z)^2 + 2\mu(-1)^j \hat{S}_j^z \right. \\ \left. - \frac{1}{\sqrt{S(S+1)}} (-1)^{\alpha'_j} \hat{S}_j^x \right] \mathcal{P}, \quad (11)$$

where $\alpha'_j = N/2$ for $j = N$ and zero otherwise. In the main text, we have dropped the phase α' , as it becomes irrelevant in the thermodynamic limit. We emphasize the importance of the projector \mathcal{P} , which effectively leads to an interaction among neighboring spins and allows us to rewrite $(1/2)\mathcal{P} (\hat{\sigma}_j^+ \hat{S}_j^+ \hat{\sigma}_{j+1}^- + \text{h.c.}) \mathcal{P} = \mathcal{P} \hat{S}_j^x \mathcal{P}$ (see also [71] for the special case of $S = 1/2$).

To find the dimension of $\mathcal{H}_{\text{phys}}$, we need to count all possible configurations allowed by Gauss' law. In the basis of \hat{S}_z , this is conveniently expressed by a square matrix C_S of size $2S + 1$,

$$C_S = \begin{pmatrix} 1 & & & & & & & \\ 1 & 1 & & & & & & \\ & 1 & 1 & & & & & \\ & & \ddots & \ddots & & & & \\ & & & 1 & & & & \\ & & & & 1 & 1 & & \\ & & & & & & 1 & 1 \end{pmatrix}. \quad (12)$$

Here, rows and columns correspond to all possible spin configurations of two neighbors and 1 or 0 indicate an allowed or forbidden pair, respectively. Gauss' law alternates between even and odd sites as expressed by the

matrices C_S and C_S^T . The total Hilbert space dimension can now be obtained by summing over all allowed configurations, which is (for periodic boundary conditions) equivalent to the following trace

$$\dim \mathcal{H}_{\text{phys}} = \text{tr} \left[(C_S C_S^T)^{N/2} \right] = \sum_j \left(x_j^{(S)} \right)^{N/2}. \quad (13)$$

The eigenvalues $x_j^{(S)}$ of the matrix

$$C_S C_S^T = \begin{pmatrix} 1 & 1 & & & \\ 1 & 2 & 1 & & \\ 1 & & 2 & & \\ & \ddots & & \ddots & \\ & & 2 & 1 & \\ & & 1 & 2 & 1 \\ & & & 1 & 2 \end{pmatrix} \quad (14)$$

are given by

$$x_j^{(S)} = 2 + 2 \cos \left(\frac{2j\pi}{4S+3} \right), \quad j = 1, \dots, 2S+1. \quad (15)$$

In summary, we proved

$$\begin{aligned} \dim \mathcal{H}_{\text{phys}} &= \sum_{j=1}^{2S+1} \left[2 + 2 \cos \left(\frac{2j\pi}{4S+3} \right) \right]^{N/2} \\ &= 2^N \sum_{j=1}^{2S+1} \left[\cos \left(\frac{j\pi}{4S+3} \right) \right]^N. \end{aligned} \quad (16)$$

In our main text and our exact diagonalization numerics, we make extensive use of the smallness of this dimension.

Analytical expressions for the vector and scalar masses

– The exact masses in the strong coupling limit ($m/e = \mu/g = 0$) are known to be

$$\frac{M_V^{(0)}}{e} = \frac{1}{2} \frac{M_S^{(0)}}{e} = \frac{1}{\pi}, \quad (17)$$

For the readers' convenience, we also quote the perturbative predictions which we used for the plots in the main text. We refer to [21] and references therein for details. Explicitly, the strong coupling expansions are given by

$$\frac{M_V + 2m}{e} = 0.5642 + 1.781 \left(\frac{m}{e} \right) + 0.1907 \left(\frac{m}{e} \right)^2 + \dots, \quad (18)$$

$$\frac{M_S + 2m}{e} = 1.128 + 3.562 \left(\frac{m}{e} \right) - 13.512 \left(\frac{m}{e} \right)^2 + \dots. \quad (19)$$

Extrapolations – As described in the main text, the ground state energy, vector, and scalar mass of the continuum Schwinger model are obtained by a series of extrapolations. From the ED, we numerically obtain the lowest three ($j = 0, 1, 2$) eigenvalues $E_j = E_j(S, N, g, m/e)$ in the zero-momentum sector of the

Hamiltonian, grouped by several values of spin length S , lattice size N , coupling $g = ae$, and mass m/e . In a first step, we rescale all quantities according to their expected behavior in the continuum limit (see e.g. [60]),

$$\omega_0(S, N, g, m/e) = \frac{g^2}{2N} E_0(S, N, g, m/e), \quad (20)$$

$$\omega_{1,2}(S, N, g, m/e) = \frac{g}{2} (E_{1,2} - E_0)(S, N, g, m/e). \quad (21)$$

Below, we indicate the step-wise extrapolation in each of the parameters S , N and g for different values of m/e . The extrapolated parameter is dropped in the list of arguments of the extrapolated function. For example, the extrapolations to large S are obtained by fitting

$$\omega_j(S, N, g, m/e) = \omega_j(N, g, m/e) + \frac{\alpha_j(N, g, m/e)}{S}. \quad (22)$$

and the extrapolated function $\omega_j(N, g, m/e)$ does not have the S -dependence any more. The $1/S$ dependence in this extrapolation is motivated as the simplest polynomial dependence on S , and also justified a-posteriori from the data. An exponential dependence would need a scale, and we have no reason to postulate the emergence of an additional lengthscale. Similarly, the large- N limit is obtained by the fits

$$\omega_0(N, g, m/e) = \omega_0(g, m/e) + \frac{\beta_0(g, m/e)}{N} + \frac{\gamma_0(g, m/e)}{N^2}, \quad (23)$$

$$\omega_{1,2}(N, g, m/e) = \omega_{1,2}(g, m/e) + \frac{\gamma_{1,2}(g, m/e)}{N^2}, \quad (24)$$

where we take into account that the leading finite size corrections of the excited states arise at second order in N [60]). Finally, we extrapolate to the continuum limit via

$$\omega_0(g, m/e) = \omega_0(m/e) + \delta_0(m/e)g + \epsilon_0(m/e)g^2, \quad (25)$$

$$\omega_{1,2}(g, m/e) = \omega_{1,2}(m/e) + \delta_{1,2}(m/e)g, \quad (26)$$

where including the second order for the ground state significantly improves the accuracy of our results, indicating that our lattice data is rather far away from the continuum limit. Our final results are the ground state energy density $\omega_0(m/e)$ and the first two energies $\omega_{1,2}(m/e)$ above the ground state. The extrapolations of the iMPS data proceed analogously, omitting the fit with respect to N .

In general, the data $\omega_j(S, N, g, m/e)$ diverges as $g \rightarrow 0$ for fixed S, N , and m/e in such a way that for every g there are minimal values of S and N required for a reliable extrapolation. In order to avoid additional assumptions about the functional form of $\omega_j(S, N, g, m/e)$, we have implemented a simple convergence check to discard data with too small values of S and N : To obtain

the results presented in the main text, we discarded all bare data corresponding to the same value of g (and fixed j) if the extrapolated values $\omega_j(N, g, m/e)$ differ by more than 10% from the value corresponding to the largest available spin length S_{\max} , i.e. when $|\omega_j(N, g, m/e) - \omega_j(S_{\max}, N, g, m/e)| > 0.1 \times |\omega_j(S_{\max}, N, g, m/e)|$. For the ED data, we checked for convergence of the N extrapolation analogously. After supplementing the fits by this procedure, and given the relatively small values of S (and N for the ED), we find that the uncertainty of all quantities is dominated by the final extrapolation to the continuum limit. The error bars shown in the plots of the main text indicate systematic errors that arise from the corresponding choice of fit range. We have estimated these errors following the procedure described in the appendix of [60].

Path integral representation – In this section, we outline a derivation of the path integral for the pure gauge $U(1)$ QLM Hamiltonian using coherent states for the quantum spin operators representing the gauge fields, and indicate how the large representations give rise to the Wilson-Kogut-Susskind limit of the gauge theory. Given a Hamiltonian H in d -spatial dimensions which satisfies a local constraint, the corresponding path integral is given by

$$\mathcal{Z} = \text{Tr} (e^{-\beta H} \mathbb{P}) = \int \mathcal{D}\Omega e^{-S[\Omega]}. \quad (27)$$

The extent in Euclidean time, β equals inverse temperature T , and \mathbb{P} is the projection operator projecting the configurations in a chosen computational basis to the ones allowed by the local constraint. The path integral is constructed by splitting the total Euclidean time β into N_t Trotter steps of extent ϵ , such that $\beta = \epsilon N_t$. At each Trotter step, we construct the transfer matrix, $\langle \Omega_{n-1} | \mathbb{T} | \Omega_n \rangle = \langle \Omega_{n-1} | \exp(-\epsilon H) | \Omega_n \rangle$, where $|\Omega_n\rangle$ denotes the computational basis (which we introduce next) at time-slices $n-1$ and n . A periodic boundary condition in the imaginary time direction for the gauge field is used. The final expression is an integral over all possible field configurations Ω in $(d+1)$ -dimensions in the limit $\epsilon \rightarrow 0$, $N_t \rightarrow \infty$ with β held fixed. Further, for $\beta \rightarrow \infty$ ground state results can be obtained.

The pure gauge Hamiltonian is given by $H_g = \frac{g^2}{2} \sum_{j=1}^N (\hat{S}_j^z)^2$, and the Gauss' law without the matter fields is simply $\hat{G}_j = \hat{S}_j^z - \hat{S}_{j-1}^z$, and in the following we will denote the projection operator which selects configurations according to this (local) constraint as $\mathbb{P}_G = \prod_j \mathbb{P}_{G_j}$. We emphasize that the fermions are not included in this Hamiltonian, and consequently the Gauss' law differs from the one in the main text. To derive the path integral, we use the coherent state basis (also known as Bloch states in the literature) as the computational basis, which is denoted as (j denotes a spatial

site, and n the timeslice)

$$\begin{aligned} |\Omega_n\rangle &= \prod_j |\theta_{j,n}, \phi_{j,n}\rangle \\ &= \prod_j (\cos \frac{\theta_{j,n}}{2})^{2S} \exp \left[\tan \left(\frac{\theta_{j,n}}{2} \right) e^{i\phi_{j,n}} S_{j,n}^- \right] |0\rangle, \end{aligned} \quad (28)$$

where $0 \leq \theta_{j,n} < \pi$ and $0 \leq \phi_{j,n} < 2\pi$. In what follows, we further need the resolution of identity in the coherent state basis at each timeslice n :

$$\mathbb{I} = \prod_j \frac{2S+1}{4\pi} \int_0^\pi \sin(\theta_{j,n}) d\theta_{j,n} \int_0^{2\pi} d\phi_{j,n} |\Omega_n\rangle \langle \Omega_n|. \quad (29)$$

Using the above expressions, in the coherent state basis, we write the partition function \mathcal{Z} as

$$\begin{aligned} \mathcal{Z} &= \int \mathcal{D}\Omega \langle \Omega_0 | e^{-\epsilon H_g} | \Omega_1 \rangle \cdots \langle \Omega_{N-1} | e^{-\epsilon H_g} | \Omega_N \rangle \\ &\quad \times \langle \Omega_N | \mathbb{P}_G | \Omega_0 \rangle \end{aligned} \quad (30)$$

The overlap $\langle \Omega_{n-1} | \Omega_n \rangle$ constitutes an important piece in the full calculation and gives rise to the Berry phase. After some algebra, it can be expressed as

$$\langle \Omega_{n-1} | \Omega_n \rangle = \exp \left[iS \sum_j \cos(\theta_{j,n}) (\phi_{j,n-1} - \phi_{j,n}) \right], \quad (31)$$

where we have assumed that ϵ is small such that the fields on adjacent time-slices are sufficiently smooth. The matrix elements of the following operators in the coherent state basis are also needed:

$$\begin{aligned} \left\langle \Omega_{n-1} \left| \sum_j \hat{S}_{j,n}^z \right| \Omega_n \right\rangle &= \langle \Omega_{n-1} | \Omega_n \rangle S \sum_j \cos(\theta_{j,n}) \\ \left\langle \Omega_{n-1} \left| \sum_j (\hat{S}_{j,n}^z)^2 \right| \Omega_n \right\rangle &= \langle \Omega_{n-1} | \Omega_n \rangle \\ &\quad \times \left[S(S - \frac{1}{2}) \sum_j \cos^2(\theta_{j,n}) + \frac{S}{2} \right]. \end{aligned} \quad (32)$$

Combining the above formulae, the transfer matrix between two time-slices is thus

$$\begin{aligned} &\langle \Omega_{n-1} | \exp(-\epsilon H_g) | \Omega_n \rangle \\ &\approx \langle \Omega_{n-1} | \Omega_n \rangle e^{-\frac{\epsilon g^2}{2} \sum_{j=1}^N S(S - \frac{1}{2}) \cos^2(\theta_{j,n}) - \frac{\epsilon g^2 S N}{2}}, \end{aligned} \quad (33)$$

where we have expanded the exponential, evaluated the operator, and re-exponentiated it, valid up to corrections

at $O(\epsilon^2)$. The last timeslice contains the projection operator, and can be written in the $|\Omega\rangle$ -basis as:

$$\begin{aligned} \left\langle \Omega_N \left| \prod_j \mathbb{P}_{\hat{G}_j} \right| \Omega_0 \right\rangle &= \left\langle \Omega_N \left| \prod_j \delta(\hat{S}_j^z - \hat{S}_{j-1}^z) \right| \Omega_0 \right\rangle \\ &= \langle \Omega_N | \Omega_0 \rangle \prod_j \int_{-\pi}^{\pi} \frac{d\varphi_j}{2\pi} \exp [i\varphi_j S(\cos \theta_{j,0} - \cos \theta_{j-1,0})] \\ &= \prod_j \int_{-\pi}^{\pi} \frac{d\varphi_j}{2\pi} \exp [iS \cos \theta_{j,0} (\phi_{j,N} - \phi_{j,0})] \\ &\quad \times \exp [i\varphi_j S(\cos \theta_{j,0} - \cos \theta_{j-1,0})]. \end{aligned} \quad (34)$$

The φ_j are the Polyakov loop phases which appear as the Lagrange multiplier enforcing Gauss' law on the last time-slice. To incorporate the Polyakov loop variables with the action, we consider the matrix elements of the Hamiltonian and the Gauss' law together on the last two timeslices:

$$\begin{aligned} &\int \frac{d\Omega_N}{4\pi} \langle \Omega_{N-1} | e^{-\epsilon H_g} | \Omega_N \rangle \left\langle \Omega_N \left| \prod_j \mathbb{P}_{\hat{G}_j} \right| \Omega_0 \right\rangle \\ &= \prod_j \frac{2S+1}{4\pi} \int_0^\pi \sin \theta_{j,N} d\theta_{j,N} \int_{-\pi}^\pi d\phi_{j,N} \\ &\quad \times e^{\left[-\frac{\epsilon g^2}{2} S(S-\frac{1}{2}) \cos^2 \theta_{j,N} - \frac{\epsilon g^2 S N}{4} + iS \cos \theta_{j,N} (\phi_{j,N-1} - \phi_{j,N}) \right]} \\ &\quad \times \prod_j \int_{-\pi}^\pi \frac{d\varphi_j}{2\pi} e^{[i\varphi_j S(\cos \theta_{j,0} - \cos \theta_{j-1,0}) + iS \cos \theta_{j,0} (\phi_{j,N} - \phi_{j,0})]}. \end{aligned}$$

We collect the terms in $\phi_{j,N}$ and perform the integral

$$\prod_j \int_{-\pi}^\pi d\phi_{j,N} e^{iS(-\cos \theta_{j,N} + \cos \theta_{j,0})\phi_{j,N}}$$

which enforces the condition $\theta_{j,0} = \theta_{j,N}$ for all the spatial lattice sites (recall that $0 \leq \theta_{j,n} < \pi$). We can use this to simplify the matrix element

$$\begin{aligned} &\int \frac{d\Omega_N}{4\pi} \langle \Omega_{N-1} | e^{-\epsilon H_g} | \Omega_N \rangle \left\langle \Omega_N \left| \prod_j \mathbb{P}_{\hat{G}_j} \right| \Omega_0 \right\rangle \\ &= \prod_j \frac{2S+1}{4\pi} \int_0^\pi \sin \theta_{j,N} d\theta_{j,N} \int_{-\pi}^\pi \frac{d\varphi_j}{2\pi} \\ &\quad \times e^{\left[-\frac{\epsilon g^2}{2} S(S-\frac{1}{2}) \cos^2 \theta_{j,N} - \frac{\epsilon g^2 S N}{4} \right]} \\ &\quad \times e^{[iS \cos \theta_{j,0} (\phi_{j,N-1} - \phi_{j,0} + \varphi_j - \varphi_{j+1})]}. \end{aligned}$$

In the limit $S \rightarrow \infty$, the effective action can be obtained by minimizing the quadratic term in $\cos \theta_{j,n}$. This gives $\theta_{j,n} \approx \frac{\pi}{2} \pm \alpha_{j,n}$, thus $\cos \theta_{j,n} \approx \cos(\frac{\pi}{2} - \alpha_{j,n}) = \sin \alpha_{j,n} \approx \alpha_{j,n}$, and $\sin \theta_{j,n} \approx 1$. The integral then becomes Gaussian, which can be performed explicitly. Further, we note that the term $\phi_{j,N-1} - \phi_{j,0} = 2\pi n_j + \Delta_t \phi_j$,

where $\Delta_t \phi_j$ is the difference in the ϕ variable across the last timeslice. Note that the the same considerations as discussed here also hold for the other timeslices, as explicitly shown in Eq. (33). In fact, it is even simpler there, since the Gauss' Law does not need to be addressed, and again the quadratic term can be extremized to obtain a Gaussian integral. The overlap of the coherent states, contributing to the Berry phase will be addressed separately.

As the analysis reveals, in the $S \rightarrow \infty$ limit, the unit vector is forced to point at the equator, with minor fluctuations (denoted by $\alpha_{j,n}$). At every time slice overlap, the $\phi_{j,n}$ proceeds on the unit sphere, and thus the term $\phi_{j,N-1} - \phi_{j,0}$ contains the total number of windings around the equator. In the large- S limit, we get

$$\begin{aligned} &\int \frac{d\Omega_N}{4\pi} \langle \Omega_{N-1} | e^{-\epsilon H_g} | \Omega_N \rangle \left\langle \Omega_N \left| \prod_j \mathbb{P}_{\hat{G}_j} \right| \Omega_0 \right\rangle \\ &\approx \sum_{n_j \in \mathbb{Z}} \sqrt{\frac{2\pi}{S(2S-1)\epsilon g^2}} e^{\left[-\frac{S}{2(2S-1)\epsilon g^2} (\varphi_j - \varphi_{j+1} + 2\pi n_j + \Delta_t \phi_j)^2 \right]} \end{aligned} \quad (35)$$

The term in the exponential is the well-known Villain form [76] of the plaquette action in the Euclidean theory. Identifying $\varphi_j - \varphi_{j+1} \sim -\partial_j A_0(0)$ and $\Delta_t \phi_j \sim \partial_t A_1(0)$, the term in the exponential is the Maxwell action, and can be interpreted as the path integral in the axial gauge. In the axial gauge, all the time-like links are set to unity, except for the ones which cross the temporal boundary. In order to bring the expression to a form which is explicitly space-time symmetric, we can perform gauge transformations to spread the A_0 field away from the boundary time-slice and into the whole space-time lattice. The Boltzmann weight of the effective action contributing to \mathcal{Z} is thus

$$e^{-\mathcal{S}_{\text{eff}}} = e^{-\frac{1}{2\epsilon g^2} \int dx dt (\partial_t A_1(x,t) - \partial_x A_0(x,t))^2}, \quad (36)$$

where we have traded n and j for t and x respectively, and $A_{0,1}$ is the vector potential for the gauge field in 2-dimensions. We have thus demonstrated that how in the limit of large- S the localization of the spin operator along the equator is responsible for the emergence of the Wilson lattice gauge theory in Euclidean space.

Next, we connect the contribution from the Berry phase term of the quantum spin operators to the presence of topological terms in the Wilson action. We note, following Coleman [49], that the Hamiltonian of the continuum massless Schwinger model in the axial gauge ($A_0 = 0$) can be written as

$$H = \int dx \left[-i\bar{\psi} \gamma^1 (\partial_1 + ig A_1) \psi + \frac{1}{2} E^2 \right], \quad (37)$$

where $\psi, \bar{\psi}$ are the fermion fields and $\gamma^{1,2}$ are the gamma matrices. In one dimension, due to the Gauss' law, the

E is not an independent operator, but can be written in terms of the charge density up to an integration constant. It was shown by Coleman [49] that the integration constant acts as a background field, has the characteristics of a periodic function and is naturally related to the topological angle. Coleman further showed that for certain special values of this topological angle, $\Theta = \pi$, the physics of the model is very different from the expected confining behavior.

In the context of QLMs, it is quite remarkable that the use of full or half-integer spin representations can induce qualitatively different behavior, at least in certain parameter regimes [9]. In particular, using the toolbox of coherent states, we can demonstrate that for large S , half-integer spin representations can give rise to the topological angle $\Theta = \pi$.

Note that this topological term is generated from the overlap of the coherent states $\langle \Omega_0 | \Omega_1 \rangle \langle \Omega_1 | \Omega_2 \rangle \cdots \langle \Omega_{N-2} | \Omega_{N-1} \rangle = \exp(iS \sum_j \omega_j[\Omega_j])$ (see Eq. (33)), which is the Berry phase in the problem. $\omega_j[\Omega_j]$ is the solid angle corresponding to the worldline (closed curve due to periodic boundary condition) of a spin at site-j as it evolves in imaginary time. While the Maxwell term, S_{eff} is independent of S in the $S \rightarrow \infty$ limit, this term is sensitive to the integer vs. half-integer nature of the spin S . To see this, note that Berry phase term can be written as [69] (we drop the spatial index

without loss of generality)

$$\omega[\Omega] = \int_0^\beta d\tau \dot{\phi} \cos(\theta_\phi) = \oint_{\phi_0}^{\phi_0} d\phi \cos(\theta_\phi). \quad (38)$$

Here, θ is treated as a function of ϕ , as the spin S traces out a path $\vec{S}(\tau)$ on the surface of the 2-sphere, S^2 . Due to the periodic boundary conditions in time, the angle ϕ_0 must come back to itself. As we argued before, in the large- S limit, the unit vector is restricted to the equator with fluctuations, which makes the phase space effectively a circle. Due to the topological nature of this term, it only matters how many windings the vector makes around the equator. Thus in the leading order, the topological term contributes as $2\pi S$. For half-integer S , this gives an effective phase π , which contributes the same way as the background field $\Theta = \pi$ in the Wilson lattice gauge theory. On the other hand, for integer values of S , the phase of 2π is irrelevant, and only the plaquette action remains.

Thus, we have shown that in the large- S limit, the half integer values of S produce the same effective action as that of the Wilson theory with a background field of π , while the integer values produce an overall phase of multiples of 2π , and no extra effects. This derivation can be straightforwardly repeated with the inclusion of fermions.